Journal of Power Sources 267 (2014) 394–404

Contents lists available at ScienceDirect

Journal of Power Sources

journal homepage: www.elsevier.com/locate/jpowsour

Selenium encapsulated into 3D interconnected hierarchical porous carbon aerogels for lithium–selenium batteries with high rate performance and cycling stability

Shaofeng Jiang, Zhian Zhang*, Yanqing Lai, Yaohui Qu, XiWen Wang, Jie Li

School of Metallurgy and Environment, Central South University, Changsha, Hunan 410083, China

HIGHLIGHTS

- Selenium was encapsulated into hierarchical porous carbon aerogels for Li–Se batteries.
- The HPCA/Se composite showed outstanding rate capability and cycling stability.
- The $LiNO_3$ modified electrolyte signally improved cycling performance for Li–Se batteries.
- The ionic liquid $PYR_{14}TFSI$ modified electrolyte signally improved coulombic efficiency.
- The HPCA/Se composite would be a promising cathode material for Li–Se batteries.

ARTICLE INFO

Article history:
Received 7 April 2014
Received in revised form
9 May 2014
Accepted 22 May 2014
Available online 2 June 2014

Keywords:
Lithium–selenium batteries
Hierarchical porous carbon aerogels
Ionic liquid modified electrolyte
High rate performance
Polyselenides

ABSTRACT

Selenium encapsulated into 3D interconnected hierarchical porous carbon aerogels (HPCA) as a carbon/selenium composite material is prepared for lithium–selenium batteries. Scanning electron microscope (SEM) and transmission electron microscope (TEM) observations show the hierarchical porous structures of the carbon aerogels and the homogeneous distribution of selenium in the composite. The performance of the HPCA/Se cathode is evaluated in lithium–selenium batteries using cyclic voltammetry, galvanostatic charge–discharge, and electrochemical impedance spectroscopy. It is found that the HPCA/Se cathode shows high rate performance, coulombic efficiency and cycling stability. The HPCA/Se cathode has a highest coulombic efficiency which is kept above 98% after 50th cycle in ionic liquid *N*-methyl-(*n*-butyl) pyrrolidinium bis(trifluoromethanesulfonyl)imide ($PYR_{14}TFSI$) modified electrolyte and retains 309 mAh g^{-1} after 100 discharge/charge cycles at a high rate of 0.5 C (337.5 mAh g^{-1}) in $LiNO_3$ modified electrolyte, respectively. Even at the current density of 5 C (3375 mAh g^{-1}), it can still maintain at a reversible capacity of 301 mAh g^{-1}. The excellent electrochemical properties benefit from the high electron conductivity and 3D interconnected hierarchical porous structures of the carbon aerogels, which contribute to disperse selenium and absorb polyselenides, and suppress the formation of residual Li_2Se layer.

1. Introduction

Lithium–sulfur (Li–S) batteries have been studied as one of the most promising systems for the next generation high-energy rechargeable lithium batteries due to their high theoretical specific capacity (1675 mAh g^{-1}) and energy density (2600 Wh kg^{-1}) [1–4]. However, lithium–sulfur (Li–S) batteries suffer from the electronically and ionically insulating nature of sulfur and the solubility of reductive polysulfides in organic electrolyte during cycling [4–8].

As a congener of sulfur, selenium being electrochemically similar to sulfur can be expected to react with lithium to generate selenides. However, compared with sulfur (5×10^{-28} S m^{-1}), selenium (1×10^{-3} S m^{-1}) has higher electrical conductivity than that of sulfur. Although the theoretical gravimetric capacity of the selenium (675 mAh g^{-1}) is lower than that of sulfur (1672 mAh g^{-1}), the theoretical volumetric capacity of selenium (3253 mAh cm^{-3} based on 4.82 g cm^{-3}) is comparable to that of sulfur (3467 mAh cm^{-3} based on 2.07 g cm^{-3}) [9–11]. The advantages of Se make it a prospective candidate for cathode material in high

* Corresponding author. Tel./fax: +86 731 88830649.
E-mail address: zza75@163.com (Z. Zhang).

http://dx.doi.org/10.1016/j.jpowsour.2014.05.116
0378-7753/

energy density lithium batteries for specific applications. However, at present, researches on lithium–selenium (Li–Se) batteries are still at a very early stage. Similar to sulfur, the selenium cathodes also face the dissolution issue of high-order polyselenides, resulting in fast capacity fading, poor cycle performance and low coulombic efficiency [10–13].

Recently, several efforts have been made to improve the electrochemical performance of lithium–selenium batteries, such as synthesized nanoselenium with various morphologies [13,14], used porous carbon interlayer [15], prepared selenium-conductive polymer composite [16], selected suitable electrolyte and binder [10,11]. Lately, Wu et al. [13] synthesized the nanoporous selenium as a cathode material with a reversible capacity of 206 mAh g^{-1} at the current density 100 mA g^{-1} after 20 cycles. In particular, the selenium/carbon composite has been considered as one of the most promising cathode materials for advanced lithium–selenium batteries, because porous carbon materials are effective to improve the electrical conductivity of selenium and restrain the solubility of lithium polyselenides [11,12]. Abouimrane et al. [9] conducted pioneering work on the use of Se/CNT composite as a cathode material with a reversible capacity of 350 mAh g^{-1} at low current density C/12 (50 mA g^{-1}) with ether-based electrolyte after 50 cycles. Although Se/CNT composite can improves the electrical conductivity of Se containing cathodes, the porous structure of the carbon electrode materials still needs optimization to obtain higher surface area, higher electrical conductivity, larger pore volume, and more abundant pore size. Recently, a highly ordered mesoporous carbon (CMK-3) [11] with a large surface area of 1386 m^2 g^{-1} and a large pore volume 1.276 cm^{-3} g^{-1} were served as the scaffold for carbon/selenium composites with excellent cycling stability. Therefore, we urgently need select versatile properties of carbon electrode materials to improve the utilization of Se and the electrochemical performance of Li–Se batteries.

Carbon aerogels (CA), as a novel and special type of carbon material, have been recognized as promising electrode materials due to their three-dimensional (3D) interconnected structure, high surface area, large pore volume, high electrical conductivity and controllable pore size [17,18]. Importantly, the unique characteristic for CA materials is the abundant micropores and mesopores [19,20]. The microspores as microcontainers for elemental Se will play a significant role in dispersing Se and absorbing the polyselenides and restraining the shuttle phenomenon, the high surface area of the micropores provides sufficient contact to the insulating Se and conveys a high electrical conductivity to the composite material. The mesoporous offer an avenue for the mass transport of Li ions during the electrochemical cycling and accommodate the polyselenides resulting from the electrochemical reactions. However, selenium encapsulated into 3D connected hierarchical porous carbon aerogels as cathode materials has been rarely reported in Li–Se batteries.

Herein, we were motivated to prepare carbon/selenium composite by a melt-diffusion strategy which selenium was encapsulated a three-dimensional interconnected hierarchically porous carbon aerogels (HPCA) with microporous walls (<2 nm) and interconnected mesoporous (10 nm). The obtained HPCA/Se composite cathodes demonstrate high rate cyclability and cycling stability. Electrochemical results exhibit an initial discharge capacity of 587 mAh g^{-1} and retains 367 mAh g^{-1} after 50 cycles at a high rate of 0.5 C. The stable cyclability and high capacities obtained at high rates of 5 C are attributed to the unique HPCA/Se electrode architecture facilitating charge transport, and the trapping of polyselenides and cycled products within the hierarchically structured meso/microporosity in the HPCA electrode materials. In addition, we have also devoted special attention to the development of new electrolyte formulations incorporating ionic liquid *N*-methyl-*N*-butyl pyrrolidinium bis(trifluoromethanesulfonyl)imide ($PYR_{14}TFSI$) as co-solvent and $LiNO_3$ as additive for lithium–selenium (Li–Se) batteries, respectively. For the first time, we demonstrated that the use of ionic liquid $PYR_{14}TFSI$ modified electrolyte and $LiNO_3$ modified electrolyte can greatly improve the coulombic efficiency as well as cycling performance. Our results demonstrate that HPCA/Se composite is a promising cathode material for high rate performance and cycling stability lithium–selenium batteries.

2. Experimental

2.1. Materials preparation

The carbon aerogels were prepared by a sol–gel process, drying technique and carbonization [19], were etched by KOH at 800 °C for 120 min using KOH:C in mass ratio of 4:1 under argon atmosphere to obtain hierarchically porous carbon aerogels (HPCA).

A 6:4 weight ratio mixture of hierarchically porous carbon aerogels (HPCA) and Se (Sigma Aldrich, 99.5%) was mixed through wet ball-milling in acetone at 800 r min^{-1} for 2 h. After evaporating acetone in air at room temperature, the HPCA–Se mixture was heated at 260 °C for 12 h with heating rate of 5 °C min^{-1} in a tubular furnace under argon atmosphere. After cooling down to room temperature, the HPCA/Se composite was obtained. The HPCA/Se composites collected were dried in an air-oven at 50 °C for 24 h.

2.2. Material characterization

The morphologies of the samples were investigated by field emission scanning electron microscopy (FESEM, Nova Nano SEM 230) and transmission electron microscopy (TEM, Tecnai G2 20ST). The elements on the surface of sample were identified by energy-dispersive X-ray spectroscopy (EDS) and scanning transmission electron microscopy (STEM, Tecnai G2 F20)/energy dispersive X-ray spectroscopy (EDX). X-ray diffraction (XRD, Rigaku3014) measurements were made with Cu Kα radiation. Thermogravimetric analysis (TGA, SDTQ600) was conducted in determining the selenium content in the composite under N_2 atmosphere at a heating rate of 5 °C min^{-1}. N_2 adsorption/desorption measurements were performed by using Quantachrome instrument (Quabrasorb SI-3MP) at 77 K. The structure of the samples was tested by Raman spectrometer (Jobin-Yvon LabRAM HR-800, Horiba).

2.3. Electrochemical measurements

The composite cathode slurry was made by mixing 80 wt.% HPCA/Se composite material, 10 wt.% carbon black and 10 wt.% sodium alginate (SA) binder in deionized water solvent. Then, the slurry was spread onto aluminum foil (20 μm), and dried at 60 °C under vacuum overnight. The pristine selenium cathode containing 45 wt.% selenium, 45 wt.% carbon black, and 10 wt.% sodium alginate (SA) binder was prepared in the same way for comparison. The dried electrodes were punched into round discs with a diameter of 1.0 cm and an active material load of about 1.5–2 mg cm^{-2}. Coin-type (CR2025) cells were assembled in an argon-filled glove box (Universal 2440/750) in which oxygen and water contents were less than 1 ppm. The basic electrolyte used was 1 M bis (trifluoromethane) sulfonamide lithium salt (LiTFSI, Sigma Aldrich) in a solvent mixture of 1,3-dioxolane and 1,2-dimethoxyethane (1:1, v/v) (Acros Organics). The two kinds of modified electrolytes were prepared by adding 0.1 M $LiNO_3$ and 50 wt.% ionic liquid *N*-methyl-*N*-butyl pyrrolidinium bis(trifluoromethanesulfonyl)imide($PYR_{14}TFSI$) into the basic electrolyte, respectively. Lithium metal was used as counter electrode and reference electrode and Celgard

2400 was used as separator. Cyclic voltammetry (CV) and electrochemical impedance spectroscopy (EIS) measurements were conducted using PARSTAT 2273 electrochemical measurement system. CV tests were performed at a scan rate of 0.2 mV s^{-1} in the voltage range of 1.0–3.0 V. EIS measurements were carried out at open-circuit potential in the frequency range between 100 kHz and 10 mHz with a perturbation amplitude of 5 mV. Galvanostatic charge/discharge tests were performed in the potential range of 1.0–3.0 V at 25 °C by using a LAND CT2001A battery-testing instrument. The cells were first discharged to 1.0 V and then the cycle number was counted. All the electrochemical tests were conducted at room temperature.

3. Results and discussion

Textural properties of HPCA and HPCA/Se composite were examined by N_2 adsorption–desorption isotherm measurements. Fig. 1 shows the N_2 adsorption–desorption isotherms and pore size distributions of HPCA and HPCA/Se composite. From Fig. 1(a), it is shown that the curve of the HPCA exhibit a typical type IV isotherm with a hysteresis loop, indicating the existence of well-developed porous structure. Fig. 1(b) depicts the pore size distribution of the HPCA and HPCA/Se composite. HPCA exhibits a bimodal pore size distribution which includes abundant micropores and mesopores, indicating hierarchical structured meso/microporosity in the HPCA. With the incorporation of Se into the 3D interconnected HPCA framework, the BET surface area, total pore volume, micropores volume and mesoporous volume of HPCA have been decreased to 267.7 $m^2\ g^{-1}$, 0.44 $cm^3\ g^{-1}$, 0.006 $cm^3\ g^{-1}$ and 0.434 $cm^3\ g^{-1}$ from 2357.1 $m^2\ g^{-1}$, 2.17 $cm^3\ g^{-1}$, 0.594 $cm^3\ g^{-1}$ and 1.576 $cm^3\ g^{-1}$, respectively. Compared with pure HPCA sample, almost all the micropores and a part of the mesopores are disappears after encapsulating Se into HPCA matrix, suggesting that the micropores and mesopores of HPCA matrix are occupied by the incorporated Se nanoparticles.

The X-ray diffraction (XRD) patterns of Se, HPCA, HPCA–Se mixture and HPCA/Se composite are shown in Fig. 2(a). For selenium, there are several peaks at 23.5° (100), 29.7° (101), 41.3° (110), 43.6° (102), 45.4° (111), 51.8° (201), 55.7° (112), and 61.5° (202), which are in good accordance with the diffraction peaks of the trigonal phase of selenium (JCPDS 06-0362) [21,22]. For pure HPCA, the presence of the broad (002) and (100) peaks in XRD pattern of HPCA sample suggests an amorphous state [19,23]. The curve of the HPCA/Se mixture shows a similar shape like the pure HPCA sample. All of the diffraction peaks of trigonal Se disappear after heating in HPCA/Se composite, which may be due to the good dispersion of selenium at a molecular level encapsulated into 3D interconnected hierarchical porous carbon aerogels. In order to observe their structure, the Raman spectra of HPCA and HPCA/Se composite were carried out as presented in Fig. 2(b). For pure HPCA sample, two peaks are observed at 1338 and 1578 cm^{-1} representing the disordered graphite (D band) and crystalline graphite (G band), respectively [24]. The intensity ratio of D and G bands (I_D/I_G) is used to evaluate the disorder in the materials. After encapsulation of Se into three-dimensional interconnected HPCA matrix, a microstructure evolution takes place for the HPCA/Se composite. The D band shifts from the 1338–1351 cm^{-1}, while the G band shifts from 1578 to 1584 cm^{-1}. The I_D/I_G ratios of HPCA and HPCA/Se composite decrease from 1.17 to 1.04, implying that the disordering of the HPCA decreases after the incorporation of Se into the pores of HPCA [25,26].

The X-Ray Photoelectron Spectroscopy (XPS) analysis was also used to obtain valuable information about the surface of HPCA/Se composite. Fig. 3(a) depicts the XPS spectrum of C 1s, a symmetrical peak at 284.5 eV corresponds well to amorphous carbon structure [19,27]. Fig. 3(b) shows the experimental and matched Se 3d spectrum. Se $3d^{5/2}$and $3d^{3/2}$ peaks located at ~55.4 and ~56.2 eV with a spin-orbit splitting of 0.86 eV are attributed to metallic selenium [10]. The C 1s and Se 3d XPS spectrum further confirm the existence of carbon and selenium in HPCA/Se composite, which is consistent with the results of XRD.

The high-magnification field emission scanning electron microscopy (FESEM) images of (a) the HPCA and (c and d) HPCA/Se composite are shown in Fig. 4, respectively. From (Fig. 4(a)), it can be seen that the HPCA materials are composed of carbon particle interconnecting each other, forming a 3D network architectural structure [19]. As shown in Fig. 4(b), it is obviously indicated that the HPCA/Se composite still keeps three-dimensional porous structure after Se encapsulated into 3D interconnected hierarchical porous carbon aerogels. Fig. 4(c) presents the morphology of the HPCA/Se composite in which selenium particles are uniformly distributed. To confirm the distribution of Se particles in HPCA matrix, the energy dispersive X-ray analysis elemental mapping of the HPCA/Se composite is shown in Fig. 4(d) and (e). From Fig. 4(d) and (e), it is indicated that selenium and carbon are the only elements present in the HPCA/Se composite and distributed uniformly across the particles. The Se content in the composite was determined to be 56.0 wt.% by thermogravimetric (TG) analysis (Fig. 4(f)).

Furthermore, in order to study the morphological and structural character of the HPCA and HPCA/Se composite, transmission electron microscopy (TEM) and high resolution transmission electron microscopy (HRTEM) are performed at various magnifications. Fig. 5 shows TEM and HRTEM images of porous HPCA (a and b) and

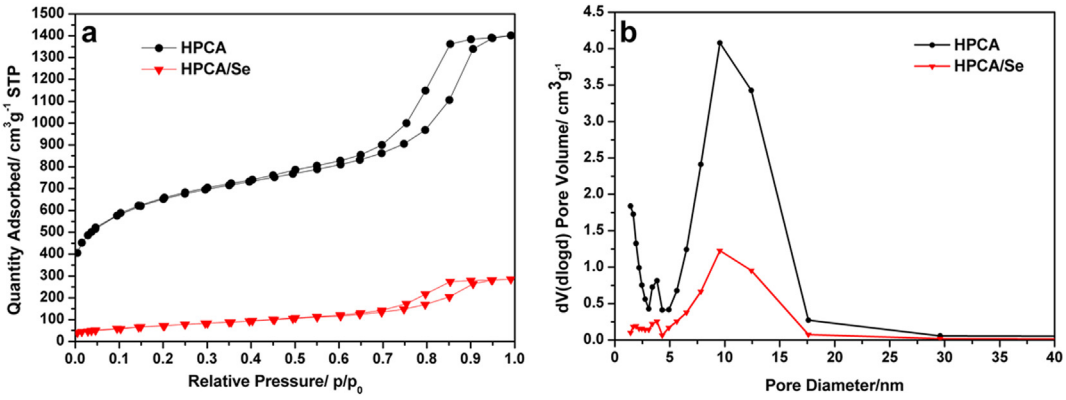

Fig. 1. (a) N_2 adsorption–desorption isotherms and (b) pore size distributions of HPCA and HPCA/Se.

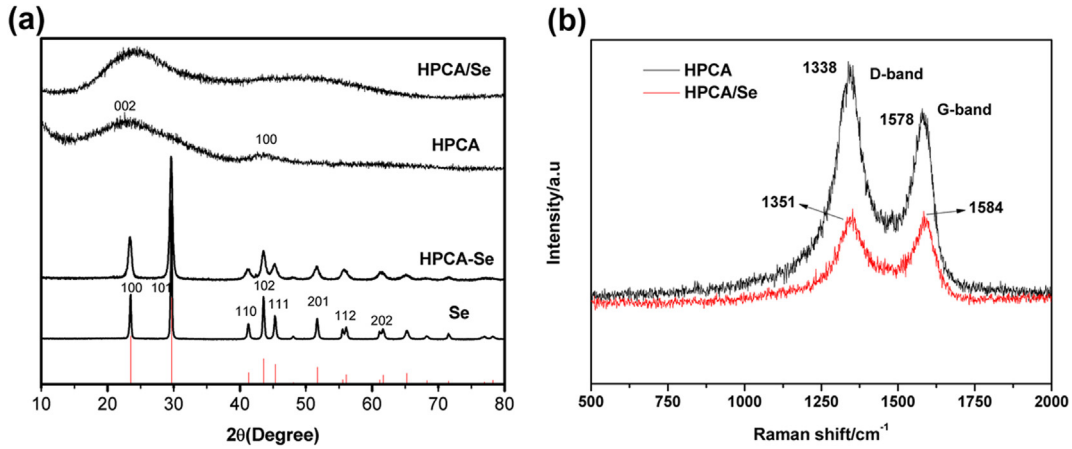

Fig. 2. (a) XRD patterns of Se, HPCA, HPCA–Se mixture and HPCA/Se composite. (b) Raman spectra of HPCA and HPCA/Se composite.

HPCA/Se composite (c, e and f). From Fig. 5(a), we can observe that the average size of HPCA particles 20 nm connected into a three dimensional conductive network. The porous structure of HPCA has typically 5–20 nm pore dimensions, and we can find abundant micropores on the surface of HPCA particles in Fig. 5(b), which are consistent with the pore size distributions pattern as shown in Fig. 1(b). Graphene-like few layers of carbon surrounding the pores of carbon can be seen at HRTEM (Fig. 5(b)) [28]. Fig. 5(c) indicates that the HPCA/Se composite can still maintains a typical interconnected product with a homogeneous distribution for Se and HPCA components. Compared with the pure HPCA sample (Fig. 5(a)), no obvious morphology change is observed after selenium is encapsulated into 3D interconnected hierarchical porous carbon aerogels, suggesting that most of the Se is filled inside the hierarchical porous carbon aerogels. The energy-dispersive X-ray spectroscopy (EDX) spectrum (Fig. 5(d)) of HPCA/Se composite demonstrates the presence of Se and C. The high magnification TEM image shown in Fig. 5(e) demonstrates the detail microstructures of the HPCA/Se composite. A high resolution TEM (HRTEM) lattice image in Fig. 5(f) of the microstructures of the HPCA/Se composite shows an arrangement of mostly disordered sp^2 carbon fringes for HPCA [19]. Compared with the pure HPCA sample (Fig. 5(b)), it is clearly revealed from Fig. 5(e) and (f) that because some of the amorphous Se phase components are entrapped within pore channels of the HPCA matrices, almost all the micropores and a part of the mesopores are filled with Se nanoparticles for the HPCA/Se composite. The microstructures revealed in Fig. 5 are in good agreement with the nitrogen adsorption–desorption isotherm characterization (Fig. 1). The energy-dispersive X-ray spectroscopy (EDS) elemental mapping images (Fig. 6) reveal that the carbon elemental mapping image overlaps with selenium mapping images, demonstrating the uniform distribution of selenium in the skeleton structure of the hierarchical porous carbon aerogels, which is consistent with the results of Fig. 5(d).

Cycling performances and coulombic efficiency of the pristine Se and HPCA/Se composite cathodes are presented in Fig. 7(a). All capacities in this study were calculated based on selenium mass and used the basic electrolyte (1 M LiTFSI in DOL/DME (1:1, v/v)). Fig. 7(a) shows the initial discharge capacity of the pristine Se cathode is 338 mAh g^{-1} at a current density of 337.5 mA g^{-1} (0.5 C), which is similar with the report of Wu et al. [13]. For the HPCA/Se composite cathode, it displays a higher utilization of active materials than the selenium cathode with the initial discharge capacity of 587 mAh g^{-1}. After 50 cycles, the HPCA/Se cathode retains a reversible capacity of 367 mAh g^{-1}, almost four times than the pristine Se, which can be attributed to good electronic properties and hierarchically structured meso/microporosity of HPCA and the good dispersion of selenium in the pores of HPCA. The reversible capacity for HPCA/Se composite cathode is better than the report of Abouimrane et al. [9]. Compared with the pristine Se cathode, the coulombic efficiency of the HPCA/Se composite cathode increases significantly from 44% to over 89% at 0.5 C after 50th cycle. The significantly increased columbic efficiency for the HPCA/Se composite cathode should benefit from hierarchically structured meso/

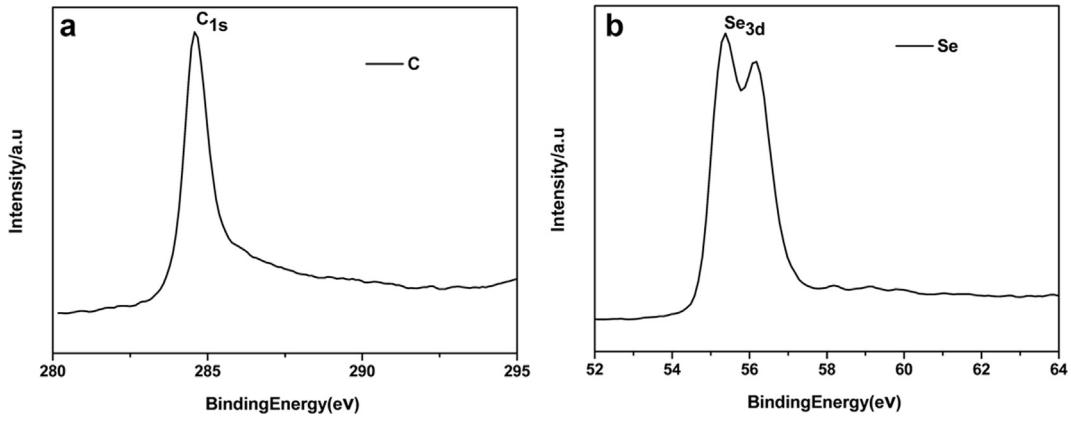

Fig. 3. XPS spectra of the HPCA/Se composite in the (a) C 1s and (b) Se 3d core region.

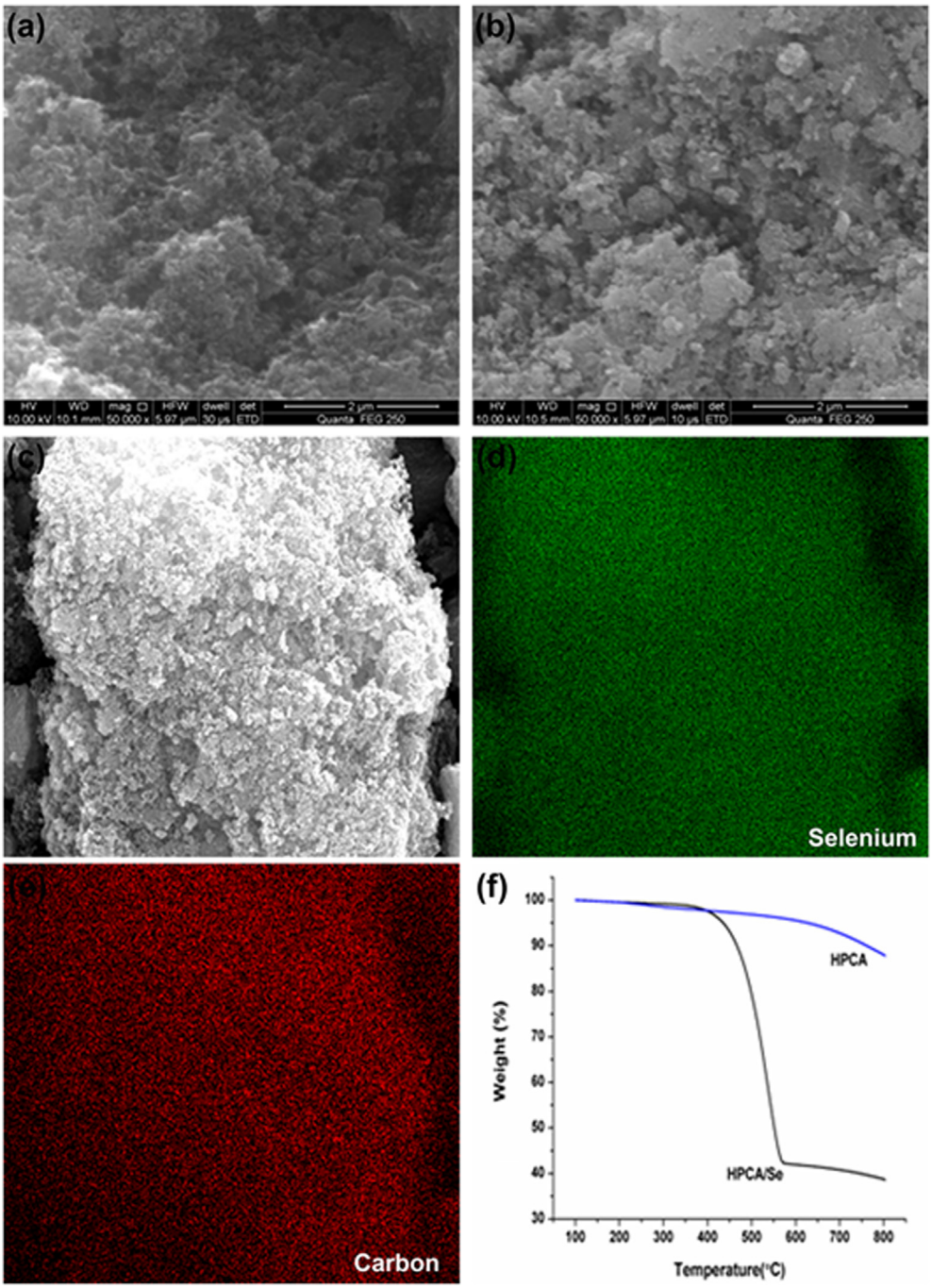

Fig. 4. SEM images of (a) HPCA, (b) and (c) HPCA/Se composite. EDS mapping of HPCA/Se composite revealing the distribution of (d) selenium and (e) carbon. (f) TGA curves of the HPCA/Se composite.

microporosity of the HPCA, the hierarchical porous structure framework can provide a physical barrier for overcharge due to alleviation of polyselenides dissolution and shuttle effect [6,23].

In order to understand the reduction/oxidation reactions in Li–Se batteries, the CVs for HPCA/Se composite cathode was recorded at a scan rate of 0.2 mV s^{-1} in the voltage range of 3.0–1.0 V with using the basic electrolyte as shown in Fig. 7(b). In the first cycle, two obvious cathodic peaks and one anodic peak were observed, which are consistent with the previous report [10,15]. The two remarkable reduction peaks for HPCA/Se composite cathode are 1.90 V and 2.14 V respectively, corresponding to the reduction of elemental selenium to soluble polyselenides and then to the insoluble Li_2Se_2 and Li_2Se [10]. In the anodic scan, only one sharp oxidation peak can be observed in the potential of 2.25 V for HPCA/Se composite cathode, which corresponds to the conversion of Li_2Se into high-order soluble polyselenides [10]. According to the result of CV, the shapes of the CV curves are close to each other and the CV peak positions are no obviously changed after first three cycles, indicating the HPCA/Se composite cathode may have the similar reversibility during the scanning.

In order to gain further insight on the electrochemical performance of the cells, galvanostatic discharge–charge test was carried out at the current density of 337.5 mA g^{-1} (0.5 C) between 1.0 V and 3 V with using the basic electrolyte. Galvanostatic

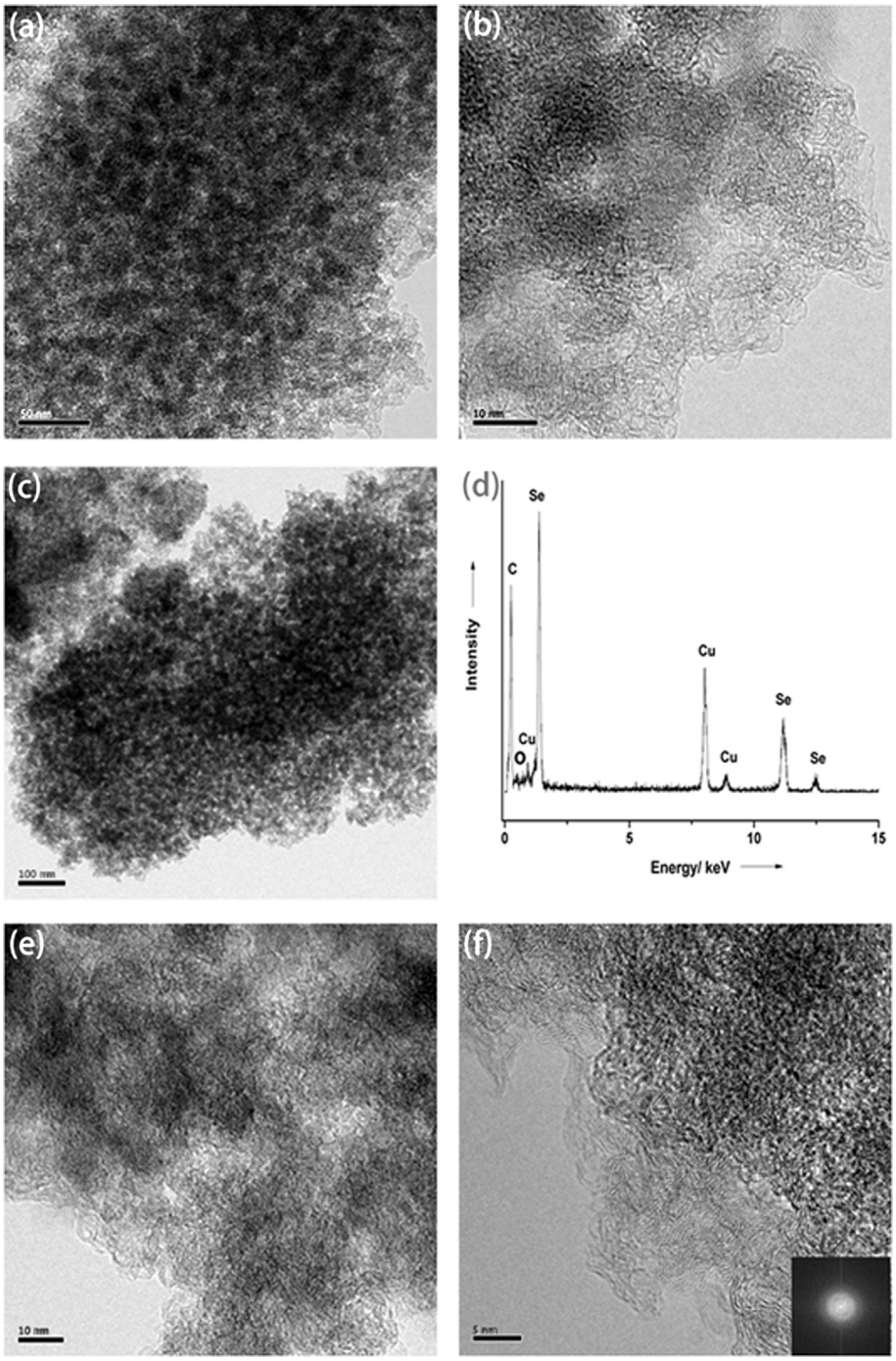

Fig. 5. TEM images of (a) HPCA, (c) and (e) HPCA/Se composite. HRTEM images of (b) HPCA and (f) HPCA/Se composite. EDX spectrum of (d) HPCA/Se composite.

discharge–charge voltage profiles of the cells with pristine Se and HPCA/Se cathodes are shown in Fig. 7(c) and (d), respectively. Consistent with the result of cyclic voltammetry measurement, two discharge plateaus are exhibited in discharge curves for both of the lithium–selenium batteries, which can be ascribed to the two step reaction of elemental selenium with metallic lithium during the discharge process [10,15]. After the 20th cycle, the pristine Se cathode discharge capacity is 185 mAh g^{-1}, showing a poor cycle performance. In contrast, the HPCA/Se composite cathode discharge capacity is 420 mAh g^{-1} after the 20th cycle having a retention rate of 72%. It is found that the cell with HPCA/Se cathodes shows more complete and stable plateaus at 2.15 V and 1.95 V. The discharge plateau of the pristine Se cathode obviously shrinks with the increasing cycle number while the HPCA/Se composite cathode has overlapping upper plateaus, indicating the excellent electrochemical stability of the HPCA/Se composite cathode [29,30].

Due to the better cycling performance, the rate capability of the HPCA/Se composite cathodes was studied as shown in Fig. 7(e) shows. After 10 cycles at a current density of 1 C (1 C is 675 mAh g^{-1}), the HPCA/Se composite cathodes shows the reversible capacity 400 mAh g^{-1}. Even after 25 cycles at a current density of 5 C (3375 mAh g^{-1}), HPCA/Se composite cathode shows good rate reversible capacity 301 mAh g^{-1}. After 30 cycles, as the

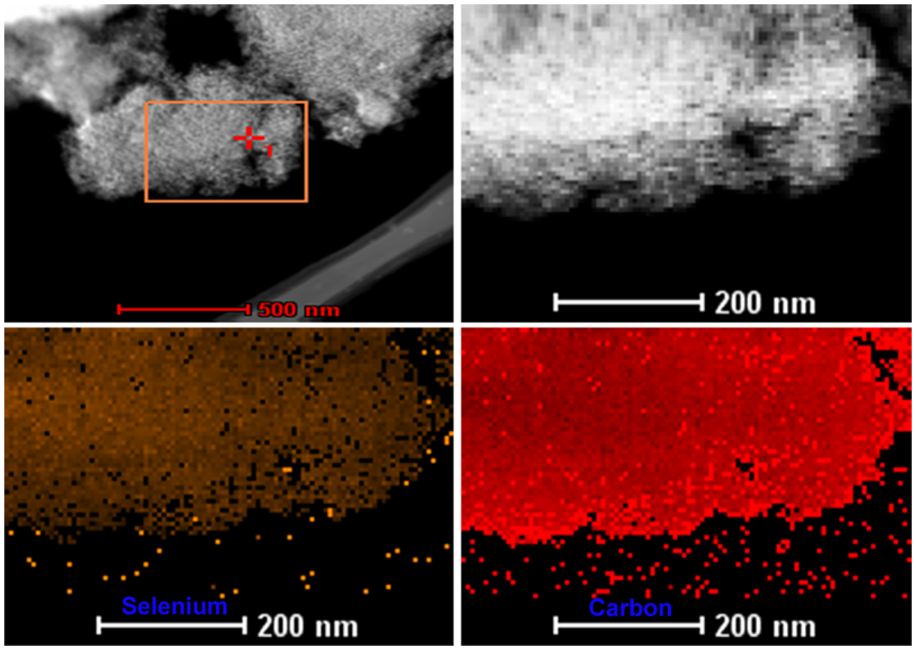

Fig. 6. EDS elemental mapping images of selenium and carbon in HPCA/Se composite.

current density returns to 0.5 C, the reversible specific capacity can remains at values of 343 mAh g^{-1}. Then, after 35 cycles, as the current density returns to 0.2 C, the reversible specific capacity can even remains at values of 406 mAh g^{-1}. The HPCA/Se composite cathode shows high rate capability, which is slightly better than the report of Guo et al. [11]. The high capacities obtained at high rates of 5 C are attributed to the unique HPCA/Se composite cathode architecture facilitating charge transport, and the trapping of polyselenides and cycled products within the hierarchically structured meso/microporosity in the HPCA electrode materials. In other words, the carbon materials can effect on improving the cycling and rate capability, which is consistent with the results of Wu [31,32].

To get further insight into the improved electrochemical performance with the use of HPCA, electrochemical impedance spectroscopy (EIS) analysis was carried out. The EIS data were obtained (Fig. 8(a)) before cycling and (Fig. 8(b)) after 50 cycles using the basic electrolyte. The impedance plots are composed of a depressed semicircle at high frequency, and an inclined line at low frequency, similar to the previous literature [10,15]. The diameter of the semicircle corresponds to the charge transfer resistance (R_{ct}) of the cell which is mainly generated at the interface between the electrode and the electrolyte. In addition, the inclined line at low frequency reflects the Li ion diffusion into the active mass. It can be seen in Fig. 8(a) that the charge transfer resistance of the cell decreases by about 50% after entrapping selenium in 3D interconnected hierarchical porous carbon aerogels. In addition, the charge transfer resistance of both cells decreases after 50 cycles. EIS characterization suggests that the charge transfer ability during the charge/discharge process is much improved by the percolating electronic path of the HPCA network. The HPCA matrices with a good electrical conductivity can serve as the conductive channels between elemental Se, which decreases the inner resistance of battery and is favorable for stabilizing the electronic and ionic conductivity, therefore leading to a higher specific capacity. The HPCA matrices contain abundant micropores which are disadvantageous to Li^+ transmission, but it is the paragon storage space for elemental Se, such the elemental Se could be highly dispersed inside the narrow micropores of HPCA matrices, which is beneficial to the excellent high rate discharge capability of the Se cathode owing to the good electrical conductivity of HPCA materials. Importantly, the narrow micropores of HPCA can trap stably elemental Se and subsequent lithium polyselenides during cycling due to such a strong adsorption, avoiding the shuttle reaction, mass loss of the active materials and the formation of the thicker Li_2Se insulating layer on the composite surface. Therefore, the electrochemical reaction constrained only inside the narrow micropores proposed here would be the dominant factor for the enhancement of the long electrochemical stability of the HPCA/Se composite cathode.

To investigate the morphological change of the cathode after the charge/discharge process, the cycled cathodes were removed from coin cells. Fig. 9 shows SEM images of (a) HPCA/Se composite and (c) and (e) the pristine Se cathodes before cycling, and the (b) HPCA/Se composite and (d) and (f) the pristine Se cathodes after cycling at 0.5 C rate for 50 cycles with using the basic electrolyte. The HPCA/Se composite cathode still maintains a relatively structural integrity and shows indistinguishable difference in morphology after cycles, implying that the electrochemical process has limited impact on the cathode structure during cycling. This result indicates that the reduction/oxidation process of the active Se is effectively localized to the 3D interconnected hierarchical porous carbon aerogels network structure. In contrast, the morphological of pristine Se cathode have an obvious structural failure after 50 cycles, which may cause by continuous loss of the active Se and gradual aggregation of irreversible insulated Li_2Se on the cathode surface. In other words, the pristine Se cathode cannot prevent the dissolution of polyselenides, resulting in poor electrochemical performance. In contrast, a HPCA/Se composite cathode, which produced by entrapment of selenium in 3D interconnected hierarchical porous carbon aerogels, not only maintains the structural integrity but also suppresses the migration of soluble polyselenides from the HPCA matrix.

The chemical constituents of the active material at different discharge/charge states were further investigated by XRD (Fig. 10). The process of pasting the electrode with SA binder has no considerable effect on the structure of Se, because the XRD signals of the electrode are the same as those of the composite (in Fig. 2(a)).

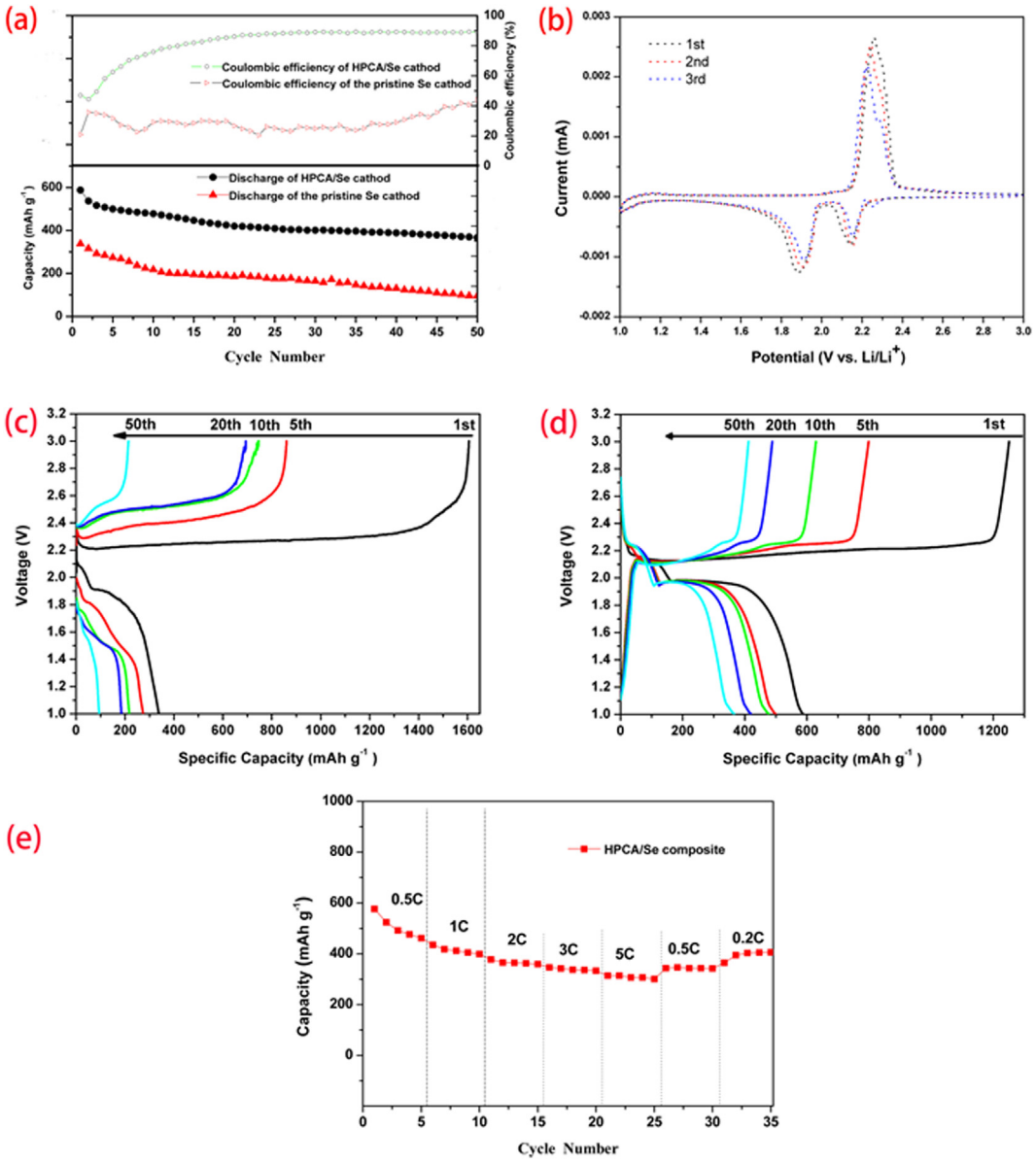

Fig. 7. (a) Cycling performance and coulombic efficiency of the pristine Se and HPCA/Se composite cathodes at 0.5 C with the basic electrolyte. (b) CV curves of the HPCA/Se composite cathode at 0.2 mV s^{-1} with the basic electrolyte. Discharge/charge curves of (c) the pristine Se and (d) HPCA/Se composite cathodes at 0.5 C with the basic electrolyte. (e) Rate performance of the HPCA/Se composite cathode with the basic electrolyte.

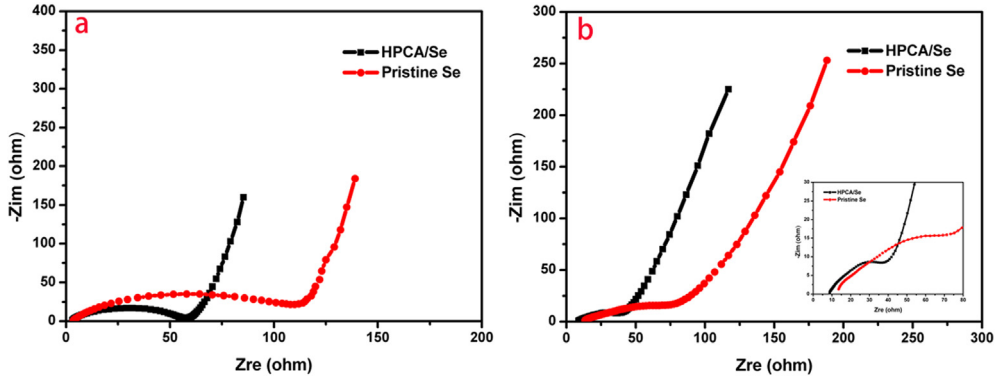

Fig. 8. Nyquist plots of the cell with the pristine Se and HPCA/Se composite cathodes with using the basic electrolyte (a) before cycling and (b) after 50th charges.

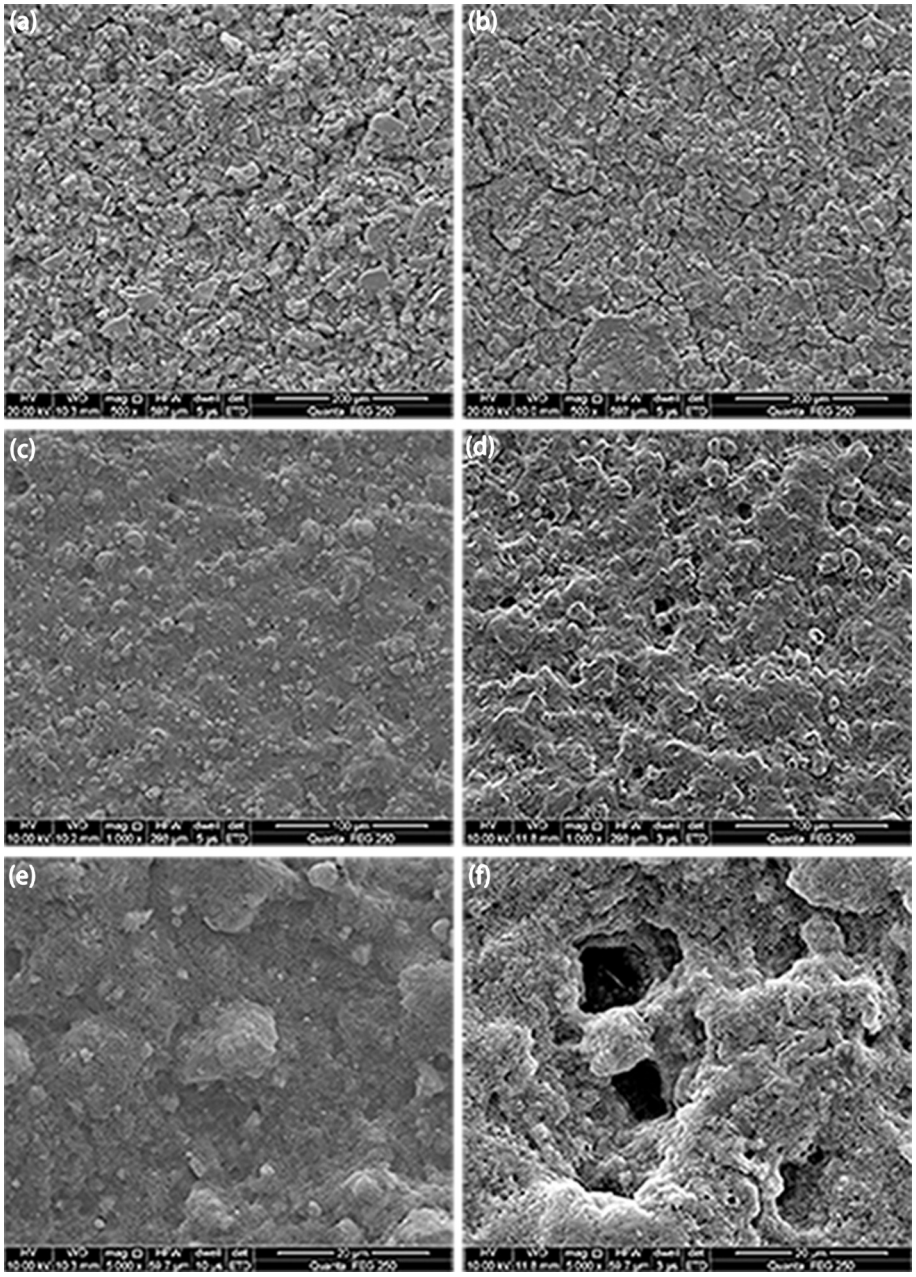

Fig. 9. SEM images of (a) HPCA/Se composite and the (c) and (e) pristine Se cathodes before cycling, the (b) HPCA/Se composite and (d) and (f) pristine Se cathodes after cycling at 0.5 C rate for 50 cycles with the basic electrolyte.

After the first discharge to 1.0 V, Se_8 reacts with Li to form Li_2Se, as confirmed by the XRD pattern. When charged, the absence of Li_2Se in the XRD pattern indicated that Li_2Se converse into high-order soluble polyselenides [12–14], which are consistent with the curves of the CV as shown in Fig. 7(b). Fig. 11 depicts the scheme of the possibility of the heating-melt process and the discharge reaction model of the HPCA/Se composite cathode. The three dimensionally networked HPCA matrices in the HPCA/Se composite serves as a useful electronic framework for elemental Se homogenous dispersion. In heating-melt process, Se nanoparticles with several nanometers may first occupy the sites of micropores, whose volume is about 27.4% of the whole porous volume of the HPCA matrix, this directly leads to a rapid decrease of the number of the micropores. While more and more Se are incorporated, almost all the micropores are occupied, then Se nanoparticles can easily enter into the position of mesopores [19], which is consistent with the results of Fig. 1. In discharge process, elemental selenium reacts with lithium to generate soluble polyselenides and then to the insoluble Li_2Se_2 and Li_2Se [10], which is consistent with the results of CV and galvanostatic discharge–charge test.

To further improve the battery performance, the modified electrolytes with $LiNO_3$ and $PYR_{14}TFSI$ were applied in the lithium–selenium batteries. $LiNO_3$ has been shown to passivate the surface of lithium anode and thus reduce the shuttle effect in lithium–sulfur (Li–S) batteries [33,34]. The ionic liquid $PYR_{14}TFSI$ as a 'co-solvent' of the electrolyte has been well known to form a protecting layer on the electrode surface during electrochemical processes and suppressed dissolution of the discharge intermediate polysulfides in the ionic liquid electrolyte with high coulombic efficiency in lithium–sulfur batteries [35,36]. Cycling performances

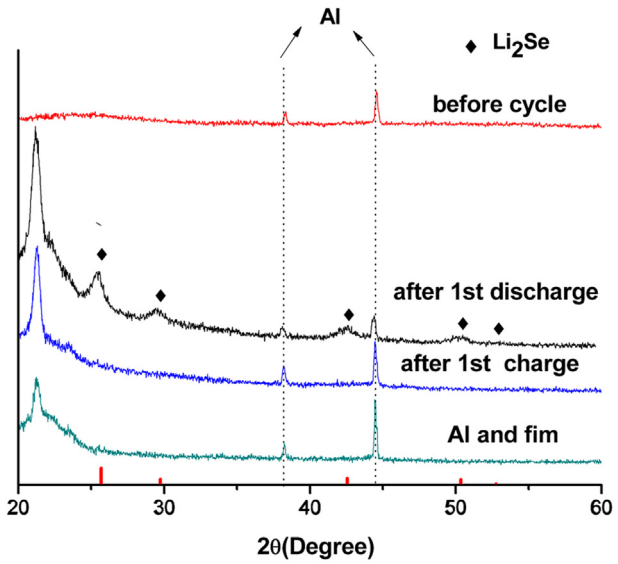

Fig. 10. XRD patterns of the HPCA/Se composite cathode with SA binder and the basic electrolyte before cycle, after the first discharge, and after first discharge/charge cycles. The base, consisting of Al foil and a film to separate the cathode from air and water, is also shown.

(a) and coulombic efficiency (b) of the two modified electrolytes for HPCA/Se composite cathode were investigated as shown in Fig. 12. Fig. 12(a) shows that the initial discharge capacity for the HPCA/Se cathode were around 650 mAh g^{-1}, 645 mAh g^{-1} and 587 mAh g^{-1} at the rate of 0.5 C (337.5 mA g^{-1}) with $LiNO_3$ modified electrolyte, $PYR_{14}TFSI$ modified electrolyte and the basic electrolyte, respectively. After 100 cycles, the HPCA/Se cathode with $LiNO_3$ modified electrolyte retains a reversible capacity of 309 mAh g^{-1}, which has a best stable reversible capacity than the both HPCA/Se cathode with $PYRth_{14}TFSI$ modified electrolyte and the basic electrolyte. More importantly, the coulombic efficiency for modified electrolytes increase significantly at 0.5 C from Fig. 12(b). Note that the HPCA/Se cathode with $PYR_{14}TFSI$ modified electrolyte has a highest coulombic efficiency which is >92% in the first cycle and kept above 98% after 50th cycle. The improvement in coulombic efficiency confirms that the addition of $LiNO_3$ and $PYR_{14}TFSI$ both may significantly reduce polyselenides reaction at the lithium anode and thus the shuttle effect in the lithium–selenium batteries.

In addition, a long-term discharge–charge test at 1 C for 300 cycles were performed for with pristine Se (basic electrolyte) and HPCA/Se cathodes as shown in Fig. 13 to further support the superior cycling stability and rate performance of the HPCA/Se cathode with $LiNO_3$ modified electrolyte. The specific capacity of this HPCA/Se cathode stabilizes around 1010.8 mAh cm^{-3}

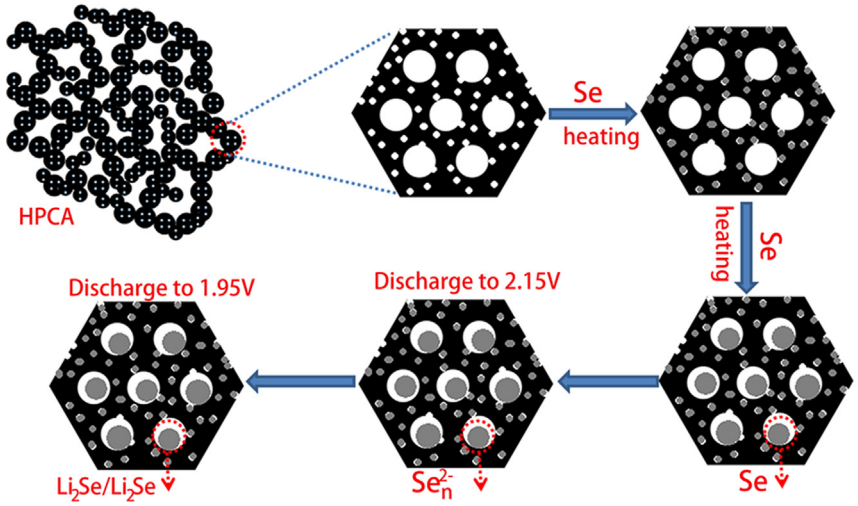

Fig. 11. Scheme of the possibility of the heating-melt process and the discharge reaction model of the HPCA/Se composite cathode.

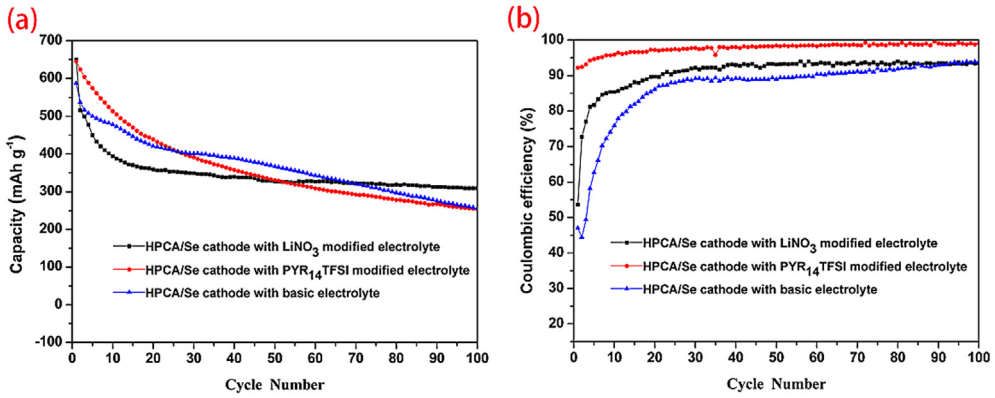

Fig. 12. (a) Cycling performance and (b) coulombic efficiency of the HPCA/Se composite cathode at 0.5 C with the basic electrolyte, $PYR_{14}TFSI$ modified electrolyte and $LiNO_3$ modified electrolyte.

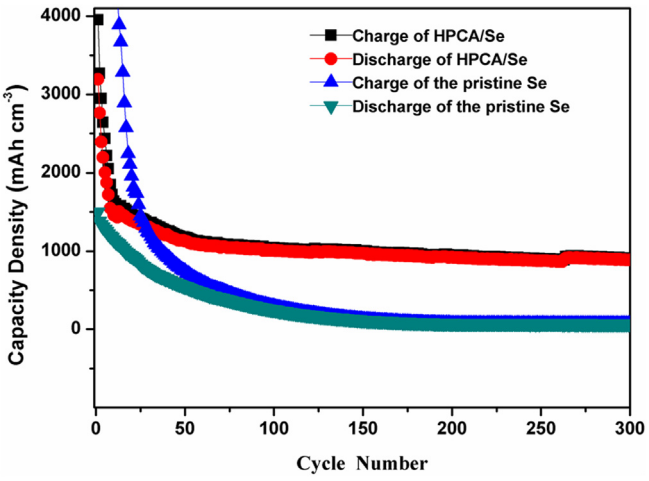

Fig. 13. Long-term cycling performances of the pristine Se (basic electrolyte) and HPCA/Se composite ($LiNO_3$ modified electrolyte) cathodes at 1 C for 300 cycles.

(209.7 mAh g^{-1}) after 100 cycles and achieves 888.3 mAh cm^{-3} (184.3 mAh g^{-1}) after 300 cycles, and its columbic efficiency retains above 98% after 100th cycle, while the pristine Se cathode retains only 70.4 mAh cm^{-3} (14.6 mAh g^{-1}). Therefore, the hierarchically structured meso/microporosity in the HPCA electrode materials improves the cycling stability of HPCA/Se composite cathode.

4. Conclusion

We synthesized HPCA/Se composite with high dispersed elemental Se inside the micropores and mesoporous of HPCA matrix by a melt-diffusion strategy. The results show that the highly conductive HPCA matrix allow fast transport of electrons and Li^+ ions, provide hierarchical porous structure to encapsulate Se and absorb polyselenides, and suppresses the shuttle effect during charge/discharge process. Hence, the HPCA/Se composite cathode exhibits superior cyclability and coulombic efficiency, high rate cyclability than the pristine Se cathode. The HPCA/Se composite cathode (using based electrolyte) with sulfur content of 56 wt.% displays an initial discharge capacity of 587 mAh g^{-1} and a reversible discharge capacity of 367 mAh g^{-1} after 50 cycles at 0.5 C charge/discharge rate, which almost four times than the pristine Se. Even at the current density of 5 C (3375 mAh g^{-1}), the HPCA/Se composite can still maintain at a reversible capacity of 301 mAh g^{-1} after 25 cycles. In addition, for the first time, we demonstrated that the use of ionic liquid $PYR_{14}TFSI$ modified electrolyte and $LiNO_3$ modified electrolyte can greatly improve the coulombic efficiency as well as cycling performance for lithium–selenium (Li–Se) batteries. The HPCA/Se cathode achieved coulombic efficiency is >92% for $PYR_{14}TFSI$ modified electrolyte in the first cycle and keeps above 98% after 50th cycle. The HPCA/Se cathode with $LiNO_3$ modified electrolyte retains 309 mAh g^{-1} after 100 discharge/charge cycles at a high rate of 0.5 C (337.5 mAh g^{-1}). Therefore, HPCA/Se composite is a promising cathode material for high rate performance and cycling stability lithium–selenium (Li–Se) batteries.

Acknowledgments

The authors acknowledge the financial support of the Teacher Research Fund of Central South University (2013JSJJ027) and Fundamental Research Funds for the Central Universities of Central South University (No. 2014zzts180).

References

[1] D. Peramunage, S. Licht, Science 261 (1993) 1029–1032.
[2] J. Nelson, S. Misra, Y. Yang, A. Jackson, Y. Liu, H. Wang, H. Dai, J.C. Andrews, Y. Cui, M.F. Toney, J. Am. Chem. Soc. 134 (2012) 6337–6343.
[3] X. Ji, K.T. Lee, L.F. Nazar, Nat. Mater. 8 (2009) 500–506.
[4] S.S. Zhang, J. Power Sources 231 (2013) 153–162.
[5] L. Yin, J. Wang, F. Lin, J. Yang, Y. Nuli, Energy Environ. Sci. 5 (2012) 6966–6972.
[6] N. Jayaprakash, J. Shen, S.S. Moganty, A. Corona, L.A. Archer, Angew. Chem. Int. Ed. 50 (2011) 5904–5908.
[7] C.S. Kim, A. Guerfi, P. Hovington, J. Trottier, C. Gagnon, F. Barray, A. Vijh, M. Armand, K. Zaghib, J. Power Sources 241 (2013) 554–559.
[8] G. He, X. Ji, L. Nazar, Energy Environ. Sci. 4 (2011) 2878–2883.
[9] A. Abouimrane, D. Dambournet, K. Chapman, P. Chupas, W. Weng, K. Amine, J. Am. Chem. Soc. 134 (2012) 4505.
[10] Y. Cui, A. Abouimrane, J. Lu, T. Bolin, Y. Ren, W. Weng, C. Sun, V. Maroni, S. Heald, K. Amine, J. Am. Chem. Soc. 135 (2013) 8047–8056.
[11] C. Yang, S. Xin, Y. Yin, H. Ye, J. Zhang, Y. Guo, Angew. Chem. Int. Ed. 52 (2013) 8363–8367.
[12] C. Luo, Y. Xu, Y. Zhu, Y. Liu, S. Zheng, Y. Liu, A. Langrock, C. Wang, ACS Nano 7 (2013) 8003–8010.
[13] L. Liu, Y. Hou, S. Xiao, Z. Chang, Y. Yang, Y.P. Wu, Chem. Commun. 49 (2013) 11515–11517.
[14] D. Kundu, F. Krumeich, R. Nesper, J. Power Sources 236 (2013) 112–117.
[15] Z.A. Zhang, Z.Y. Zhang, K. Zhang, X. Yang, Q. Li, RSC Adv. 4 (2014) 15489–15492.
[16] L.L. Liu, Y.Y. Hou, Y.Q. Yang, M.X. Li, X.W. Wang, Y.P. Wu, RSC Adv. 4 (2014) 9086–9091.
[17] N.P. Liu, J. Shen, D. Liu, Electrochim. Acta 97 (2013) 271–277.
[18] J.C. Wang, S. Kaskel, J. Mater. Chem. 22 (2012) 23710–23725.
[19] Z.W. Zhang, Z.Q. Li, F.B. Hao, X.K. Wang, Q. Li, Y.X. Qi, R.H. Fan, L.W. Yin, Adv. Funct. Mater. 24 (2014) 2500–2509.
[20] S.F. Jiang, Z.A. Zhang, X.W. Wang, Y.H. Qu, Y.Q. Lai, J. Li, RSC Adv. 3 (2014) 16318–16321.
[21] X.M. Li, Y. Li, S.Q. Li, W.W. Zhou, H.B. Chu, W. Chen, I.L. Li, Z.K. Tang, Cryst. Growth Des. 5 (2005) 911–916.
[22] B. Cheng, E.T. Samulski, Chem. Commun. 16 (2003) 2024–2025.
[23] Y.h. Qu, Z.A. Zhang, X.W. Wang, Y.Q. Lai, Y.X. Liu, J. Li, J. Mater. Chem. A 1 (2013) 14306–14310.
[24] S. Evers, L.F. Nazar, Chem. Commun. 48 (2012) 1233–1235.
[25] J.C. Guo, Y.H. Xu, C.S. Wang, Nano Lett. 11 (2011) 4288–4294.
[26] X.F. Wang, X.P. Fang, X.W. Guo, Z.X. Wang, L.Q. Chen, Electrochim. Acta 97 (2013) 238–243.
[27] H. Ago, T. Kugler, F. Cacialli, W.R. Salaneck, M.S.P. Shaffer, A.H. Windle, R.H. Friend, J. Phys. Chem. B 103 (1999) 8116–8121.
[28] W. Weng, V.G. Pol, K. Amine, Adv. Mater. 25 (2013) 1608–1615.
[29] W. Bao, Z.A. Zhang, C.K. Zhou, Y.Q. Lai, J. Li, J. Power Sources 248 (2014) 570–576.
[30] Y.S. Su, A. Manthiram, Electrochim. Acta 77 (2012) 272–278.
[31] W. Tang, Y.S. Zhu, Y.Y. Hou, L.L. Liu, Y.P. Wu, K.P. Loh, H.P. Zhang, K. Zhu, Energy Environ. Sci. 6 (2013) 2093–2104.
[32] Q.T. Qu, Y.S. Zhu, X.W. Gao, Y.P. Wu, Adv. Energy Mater. 2 (2012) 950–955.
[33] G.Y. Zheng, Y. Yang, J.J. Cha, S.S. Hong, Y. Cui, Nano Lett. 11 (2011) 4462–4467.
[34] X. Liang, Z.Y. Wen, Y. Liu, M.F. Wu, J. Jin, H. Zhang, X.W. Wu, J. Power Sources 196 (2011) 9839–9843.
[35] J.M. Zheng, M. Gu, H.H. Chen, P. Meduri, M.H. Engelhard, J.G. Zhang, J. Liu, J. Xiao, J. Mater. Chem. A 1 (2013) 8464–8470.
[36] N. Schweikert, A. Hofmann, M. Schulz, M. Scheuermann, S.T. Boles, T. Hanemann, H. Hahn, S. Indris, J. Power Sources 228 (2013) 237–243.